

Effect of MDI–BDO hard segment on pyridine-containing shape memory polyurethanes

Shaojun Chen · Jinlian Hu · Haitao Zhuo ·
Shiguo Chen

Received: 10 January 2011 / Accepted: 12 March 2011 / Published online: 25 March 2011
© Springer Science+Business Media, LLC 2011

Abstract Shape memory polymers are attractive for both science and industrial application. In this article, a series of pyridine-containing supramolecular shape memory polyurethanes (Py-SMPUs) with various diphenylmethane diisocyanate–butanediol (MDI–BDO) contents are synthesized from the 1,6-hexamethylene diisocyanate (HDI), *N,N*-bis(2-hydroxyethyl) isonicotinamide (BINA), BDO, and MDI. Then, they are investigated systematically using FT-IR, DSC, DMA, WAXD, and shape memory testing. The results show that the addition of MDI–BDO segment improves the strength of hydrogen bonding of Py-SMPUs. It promotes the formation of hard domains, but not influences the phase-separation structure, the intensity, and distribution of physical netpoints. In addition, the MDI–BDO segment improves the rubber modulus and drops the energy loss of Py-SMPUs. However, it does not influence the shape memory behaviors which are mainly influenced by the BINA content. If the BINA content is beyond 30 wt%, good shape memory effect can be achieved in the BINA–HDI–BDO–MDI system; and high shape recovery force can be obtained by increasing the MDI–BDO segment.

Introduction

Shape memory polymers (SMPs) have been widely studied for both academic and industrial applications in the past decades [1, 2]. Examples of SMPs include trans-polyisoprene, poly (styrene-co-butadiene), polynorbornene, and polyurethane [3–6]. Particularly, segmented shape memory polyurethane (SMPU) has been extensively researched because of their superior material properties and excellent shape memory properties, arising from the phase-separation structure [7]. The segmented SMPU is usually composed of soft segment and hard segment. The hard segments form physical netpoints, serving as the fixing phase while the soft segments form soft phase, serving as the reversible phase in the shape memory effects (SMEs). Therefore, SMEs can be controlled by adjusting the length of soft segment (SSL), the hard segment content (HSC), the molecular weight, and the preparation process [5, 8].

In the previous literature, numerous studies are concentrated on the investigations of effect of soft segment and hard segment on the SMPU [9–17]. For example, Kim [16] had studied the structure–property relationship of SMPUs in terms of various structural parameters including soft segment type and content, hard segment type and content, ionomer content, and extent of phase separation. Ji et al. had studied systematically the morphology and SMEs of segmented SMPU with crystalline reversible phase. It was found that the shape fixity of segmented SMPU decreased with the increase of HSC. The segmented SMPU having no hard segment domains showed over 90% shape recovery, and the segmented SMPU having isolated hard segment domains showed better shape recovery, while the segmented SMPU having interconnected hard segment domains showed dramatically decreased shape recovery [7]. In addition, Li. et al. [17] had investigated the crystallinity

S. Chen (✉) · S. Chen
Shenzhen Key Laboratory of Special Functional Materials,
College of Materials Science and Engineering,
Shenzhen University, Shenzhen 518060, China
e-mail: chenshaojun2@163.com

J. Hu · H. Zhuo
Institute of Textiles and Clothing, Hong Kong Polytechnic
University, Hung Hom, Hong Kong, China

and the formation of hard segment of PCL–MDI–BDO system SMPUs. Chen et al. [12] had investigated the effect of SSL and HSC on the morphology and properties of PHA–MDI–BDO system SMPUs. Chun et al. [18] had studied the effect of glycerol cross linking and HSC on the SMEs of SMPUs. Mondal and Hu had studied the influence of hard segment and PEG 3400 on the SMEs of PTMG–MDI–BDO system SMPUs [19]. Ping et al. [20] had studied the influence of various hard segments on two-phase structure and SMEs of PCL–MDI–BDO system SMPUs as well as PLA–MDI–BDO system SMPUs [21]. Zhu et al. [22] had studied the effect of soft segment crystallization and hard segment physical crosslink on the SMEs of segmented SMPU ionomers. These studies greatly promote our understanding about the relationship between structure and morphology with the SMEs of segmented SMPUs. It also stimulates the scientists to develop actively new kinds of SMPs.

Recently, supramolecular polymers have drawn increasing attentions of scientists. Supramolecular SMPs have been developed and widely studied [23–26]. In this system, the thermal reversible switching of supramolecular networks based on the non-covalent interactions has been introduced to control the shape fixing and shape recovering. For example, Li et al. [24] had reported the SMEs in the supramolecular polymer networks containing only a small fraction (ca. 2 mol%) of ureidopyridinone (UPy) pendent side-groups, serving as the molecular switch. Zhang et al. had studied a series of supramolecular SMPs networks based on the cyclodextrin (CD) inclusion complex, serving as the physical netpoints [23, 25]. Zhu et al. had synthesized a novel kind of supramolecular SMPU with self-complementary quadruple hydrogen bonding in soft segments [26]. Most recently, we had also synthesized another kind of supramolecular SMPUs containing pyridine moieties from 1,6-hexamethylene diisocyanate (HDI), *N,N*-bis(2-hydroxyethyl) isocyanide (BINA), and 1,4-butanediol (BDO) [27]. In addition to the thermal-induced SMEs, moisture-sensitive SMEs were also achieved in this kind of pyridine-containing SMPUs (Py-SMPUs) [27–29]. The supramolecular structure and the effect of BINA content of BINA–HDI–BDO system have been investigated systematically in the previous literature [27, 29, 30]. It was reported that the hydrogen bonding in the urethane groups provides the polymer with a suitable elastic network acting as the physical netpoints, while the high fraction of hydrogen bonding in the pyridine ring serves as the molecular switch. Py-SMPUs with higher BINA content show higher shape fixity, higher shape recovery, and better strain stability [29]. However, it is difficult to distinguish the soft segment and hard segment, and the shape recovery gets weak as the BIAN content decreases in the BINA–HDI–BDO system. It is suggested that the aggregation of

physical netpoints or hard domains should be improved in the Py-SMPUs.

MDI–BDO segment which is the reaction product of diphenylmethane diisocyanate (MDI) and BDO is the most widely used hard segment of polyurethane. In addition to the hydrogen bonding, there are also dipole–dipole interaction and induced dipole–dipole interaction among the MDI–BDO hard segment [31, 32]. Therefore, MDI–BDO hard segment is used to improve the aggregation of hard domain of Py-SMPUs. A series of MDI–BDO-based Py-SMPUs (MB-PUPys) are synthesized from the BINA, HDI, BDO, and MDI in this study. The structure and morphology as well as SMEs of MB-PUPys are investigated systematically using the FT-IR, DSC, DMA, WAXD, and shape memory testing etc.

Experimental part

Materials

Extra-pure grade HDI, BDO, BINA, and MDI (all from Sigma-Aldrich Chemical Co, St. Louis, MO) were used directly. Dimethylformamide (DMF) (from Ajax Finechem Ltd, Auckland, New Zealand) was dehydrated with 4-Å molecular sieves for several days before its use as a solvent.

Synthesis of MDI-PUPy

The composition and codes of each sample are provided in Table 1; and Scheme 1 presents the synthesis routine of MB-PUPys. Typically, the reaction was carried out in a 500-mL flask filled with nitrogen and equipped with a mechanical stirrer, a thermal meter, and a condenser. First, BINA powder and DMF were added to the flask according to the composition. After dissolving the BINA powder under the mechanical stirring, an equal molar HDI was added to the flask. Second, the oil temperature was raised to about 50 °C; 0.02 wt% catalyst (Dibutyltin dilaurate) was added to the reaction. During the reaction process, 10 mL DMF each time was added to the reaction to control the viscosity of solution occasionally. After 2 h, MDI and BDO were added to the reaction, and the reaction was kept for another 4 h at 60 °C. Finally, the polymer solution diluted to 10 wt% solution was obtained. After casting on the PTFE mould and putting on the 100 °C oven for 12 h, films of MB-PUPys with different MDI–BDO contents were prepared. Before testing, all films were dried on the 100 °C vacuum again for 12 h. Sample used in this study was coded as PUPyMB**, where the “**” delegates the MDI–BDO content, e.g., PUPyMB15.

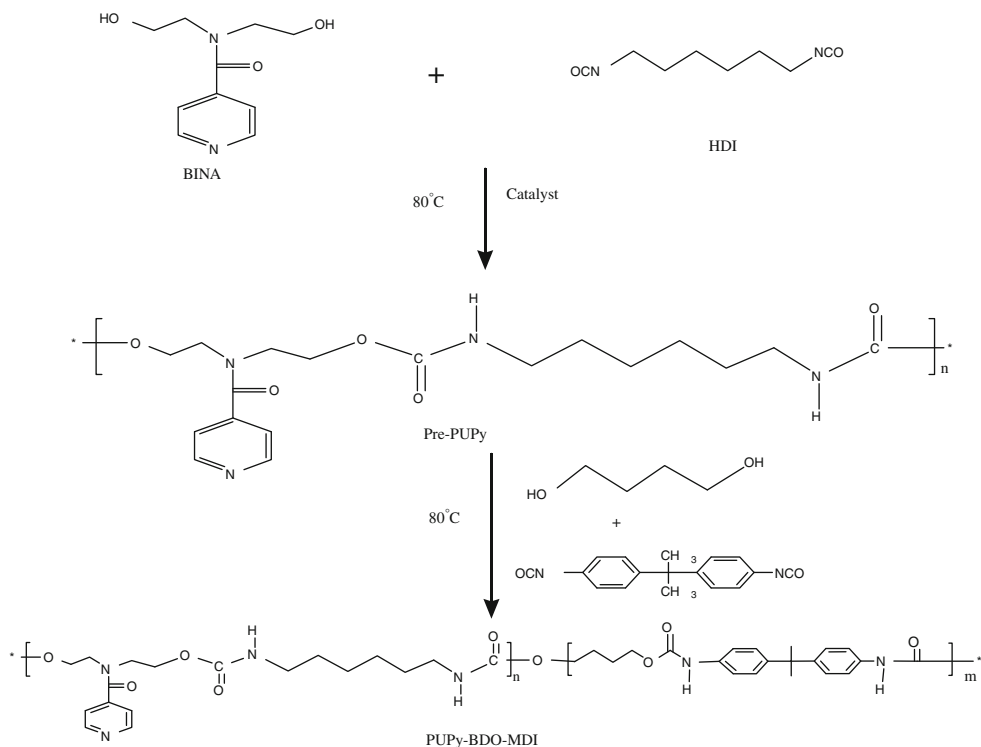
Table 1 Composition of MB-PUPys with various MDI–BDO contents

Samples	BINA (g)	HDI (g)	BDO (g)	MDI (g)	BINA wt%	MB wt%	$M_n (\times 10^4)$	PDI
PUPyMB0	5.24	4.52	0	0	53.7	0	15.38	1.63
PUPyMB15	5.24	4.52	0.46	1.29	45.5	15.2	12.37	140
PUPyMB25	5.24	4.52	0.86	2.38	40.3	24.9	19.51	1.311
PUPyMB35	5.24	4.52	1.39	3.86	34.9	35.0	11.76	1.40
PUPyMB45	5.24	4.52	2.12	5.87	29.5	45.0	10.40	1.44
PUPyMB55	5.24	4.52	3.17	8.74	24.2	55.0	8.53	1.51

M_n is the number-average molecular weight; PDI is the polydispersity index

BINA wt% is the weight fraction of BINA, which is calculated by $W_{\text{BINA}}/W_{\text{total}} \times 100\%$

MB wt% is the weight fraction of MDI + BDO, which is calculated by $(W_{\text{MDI}} + W_{\text{BDO}})/W_{\text{total}} \times 100\%$

Scheme 1 Synthesis routine for MB-PUPys

Characterization

FT-IR spectra were recorded with a Nicolet 760 FT-IR spectrometer. Ten scans at 4 cm^{-1} resolution were signal averaged and stored as data files for further analysis; smooth polymer film with a thickness of 0.2 mm was scanned by the FT-IR attenuated total reflection (ATR) method.

DSC testing was carried out using Perkin-Elmer DSC-7 at a heating rate of $10.0 \text{ }^{\circ}\text{C}/\text{min}$ and a cooling rate of $10.0 \text{ }^{\circ}\text{C}/\text{min}$ under N_2 .

WAXD traces were recorded with a scan speed of $0.02^\circ/\text{min}$ in the X-ray Diffractometer (Philips Xpert XRD System) at 40 kV and 40 mA , which was equipped with Goebel mirror and $\text{Cu K}\alpha$ radiation with a wavelength of 1.54 \AA .

In the dynamical mechanical analysis (DMA), specimens were cut from film with thickness of 0.2 mm, and the distance between two clamps was 15 mm in the initial testing status. Specimens were determined using a Perkin-Elmer DMA at 1.0 Hz with a heating rate of 3.0 K/min .

Tapping-mode atomic force microscopy (AFM) was used to visualize the images of SMPU on a DI Nanoscope IIIa AFM, operated at ambient with a double-vibration isolation system.

Thermal-induced SMEs were characterized with thermal-mechanical testing, which was done using an instron 4466 apparatus with a temperature-controlled chamber; a personal computer was used to control and record all date [12]. The standardized film size was $5 \times 20 \text{ mm}^2$, and the thickness was 0.2 mm. Specimens were firstly heated to

$T_{\text{high}} = 70^\circ\text{C}$ within 600 s (s). Then, the sample was stretched to $\varepsilon_m = 100\%$ elongation at T_{high} with 10 mm/min stretching rate. After that, cool air was introduced to the chamber for cooling sample film with constant strain $\varepsilon_m = 100\%$ elongation to $T_{\text{low}} = 20^\circ\text{C}$ within 900 s. Thereafter, the strain was released from ε_m to 0, and the temperature was recurrent raised to 80 °C for 600 s. That was one cycle among all cyclic tensile tests. The cycle for each sample was repeated four or five times for assessing the thermal-induced SMEs. Finally, the shape fixity (R_f) and shape recovery (R_r) were calculated according to the method of literature [29, 33].

Thermal-strain recovery testing was performed in a microscopy (Leitz Wetzlar) with a hot stage (Mettler Toledo FP90 Central Processor & FP82 Hot Stage) and a camera (Pixera PVC 100C). The heating rate of the recovery measurement was 2 °C/min; the length of specimen was recorded on heating process within the temperature range of 25–100 °C. Then, the shape recovery at any temperature (R_T), the final recovery rate (R_f), and shape fixity (F) were calculated according to the method of literature [29, 34].

Results and discussions

FT-IR analysis

Figure 1 presents the FT-IR spectra of MB-PUPys with various MDI–BDO contents. According to the previous literature[30], similar to the BINA–HDI–BDO system, it is known that the frequencies at about 3317 and 1696 cm^{-1} are assigned to the stretching vibration of N–H of urethane group and stretching vibration of C=O of urethane, respectively. They delegate the formation of urethane groups. The frequency at 1635 cm^{-1} is assigned to the stretching vibration of the C=O group beside the pyridine ring. The frequency at 3058 cm^{-1} is attributed to the C–H stretching vibration of the pyridine ring. The frequencies at 2932 and 2858 cm^{-1} are attributed to out-of-phase asymmetric CH_2 stretching and in-phase asymmetric CH_2 stretching, respectively. The frequencies at 1532 and 1239 cm^{-1} are assigned to C–N stretching vibration of urethane groups. The frequencies at about 998 and 832 cm^{-1} are assigned to the pyridine ring [30]. In Fig. 1, it is observed that the peak intensity at 1596 cm^{-1} increases with the increase of MDI–BDO content. It means that the fraction of hydrogen bonding in the urethane groups increases with the MDI–BDO content. In addition, it is found that the frequency at about 1239 cm^{-1} in the PUPyMB0 without MDI–BDO segment shifts to lower frequency at about 1232 cm^{-1} in the PUPyMB25, at about 1220 cm^{-1} in the PUPyMB35, PUPyMB45, and PUPyMB55. It indicates that the strength of

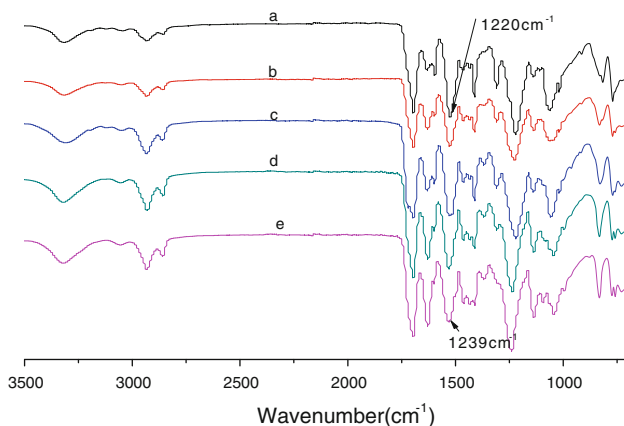


Fig. 1 FT-IR spectra of MB-PUPys with various MDI–BDO contents (a): PUPyMB55; (b): PUPyMB45; (c): PUPyMB35; (d):PUPyMB25; and (e):PUPyMB0

hydrogen bonding in the urethane groups is improved when the MDI–BDO segment is introduced to the HDI–BINA system, e.g., BINA–HDI–BDO–MDI system. This structure is the foundation for the aggregation of hard segments or the formation of stable hard domains.

DSC analysis

In an earlier report, the thermal properties of BINA–HDI–BDO system have been investigated [29]. It was reported that slight glass transition and broad high temperature transition appeared on the first heating curves of BINA–HDI–BDO system. When the BINA content was lower than 30 wt%, crystal melting temperatures were even found within high temperature range [29]. However, when the MDI–BDO segment is introduced to the BINA–HDI–BDO system, more rigid MDI–BDO hard domain will be formed in the BINA–HDI–BDO–MDI system [12]. The aggregation of relatively regular HDI–BDO unit will be interrupted by the irregular MDI–BDO unit due to the strong molecular interaction [32]. Thus, the thermal properties of BINA–HDI–BDO–MDI system should be different from that of BINA–HDI–BDO system.

Figure 2 presents the first DSC heating curves and the second DSC heating curves of MB-PUPys with various MDI–BDO contents. It is observed in Fig. 2a that a broad high temperature with a big ΔC_p is observed within the temperature range of 83–120 °C on the first heating curves while there is no crystal melting peak in all the samples, even the sample PUPyMB0. However, the endothermic transition disappears when the specimen undergoes the second scan. Robert and Stuart suggested that the endothermic transitions observed at about 120 °C were correlated with the long-range hard segment units [35]. It implies that the long-range hard domains are formed, and

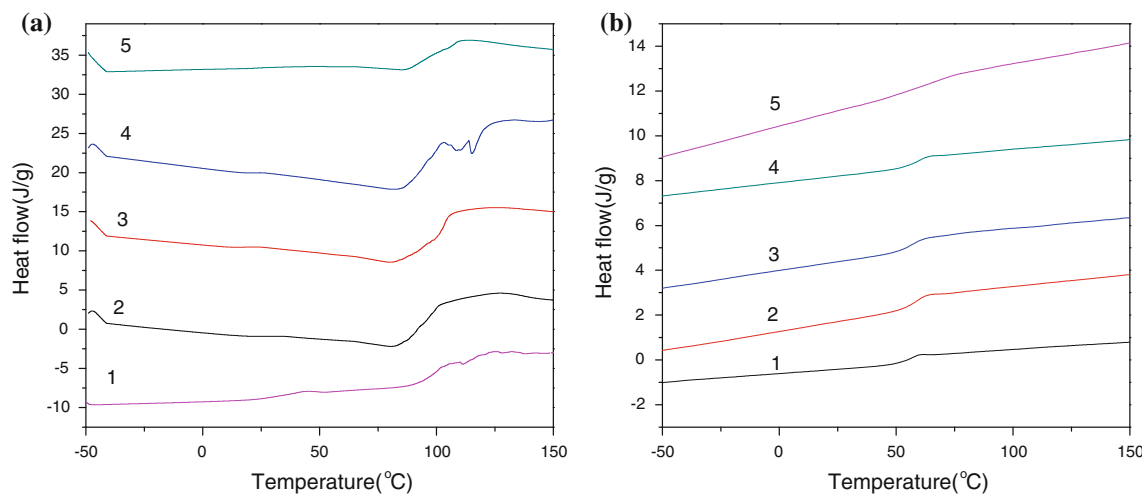


Fig. 2 **a** The first and **b** the second DSC heating curves of MB-PUPys with various MDI–BDO contents: **1** PUPyMB0; **2** PUPyMB15; **3** PUPyMB25; **4** PUPyMB35; and **5** PUPyMB45

the formation of hard domains requires a long time self-assembly process in the BINA–HDI–BDO–MDI system. In addition, it is observed in Fig. 2b that a clear glass transition is determined within the low temperature range on the second heating curves. As the MDI–BDO content increases, the glass transition temperature (T_g) shifts to higher temperature. This result is very consistent with the results observed in the common SMPU-like PHA-based SMPU [12]. However, on the other hand, the T_g increases with the decrease of BINA since the increase of MDI–BDO content results in the decrease of BINA content in the BINA–HDI–BDO–MDI system. It is not consistent with the results observed in the BINA–HDI–BDO system, in which the T_g of soft phase increases with the decrease of BINA content [29]. This is due to the fact that the increased MDI–BDO hard segment not only improves the interaction of polymer, but also improves the rigid of polyurethane chain [12]. It implies that the MDI–BDO segment have great influence on the movement of polymer chain in the BINA–HDI–BDO–MDI system. Thus, it is known from the DSC results that phase-separation structure consisting of amorphous soft phase and amorphous hard phase occurs in the BINA–HDI–BDO–MDI system. The hard phase is formed on the basis of the aggregation of long-range disordered urethane unit through the hydrogen bondings. The addition of MDI–BDO segment does promote the formation of hard domains.

WAXD analysis

Figure 3 presents the WAXD trace of MB-PUPys with various MDI–BDO contents. In the previous literature, it was reported that the HDI–BDO hard segment did not form crystalline phase until the content of HDI–BDO was higher

than a critical value, e.g., above 28.6 wt% in the PLA3000-based polyurethane, above 19.4 wt% in the PLA5000-based polyurethane, and above 10.7 wt% in the PLA10000-based polyurethane [36]. In the BINA–HDI–BDO system, it was reported that the HDI–BDO segment cannot form crystalline hard phase until the HDI–BDO content is higher above 65 wt%, i.e., the BINA content is less than 35% [29]. However, when the MDI–BDO segment is introduced to the BINA–HDI–BDO system, it is found in Fig. 3 that no diffraction peaks can be determined in all the specimens though PUPyMB15, PUPyMB25, and PUPyMB35 contains more than 39 wt% HDI–BDO content. It is confirmed that both the soft phase and hard phase are amorphous, and the aggregation of relatively regular HDI–BDO unit is interrupted by the irregular MDI–BDO unit in the BINA–HDI–BDO–MDI system. This result is very consistent with the DSC testing results. In addition, it is found in Fig. 3 that the

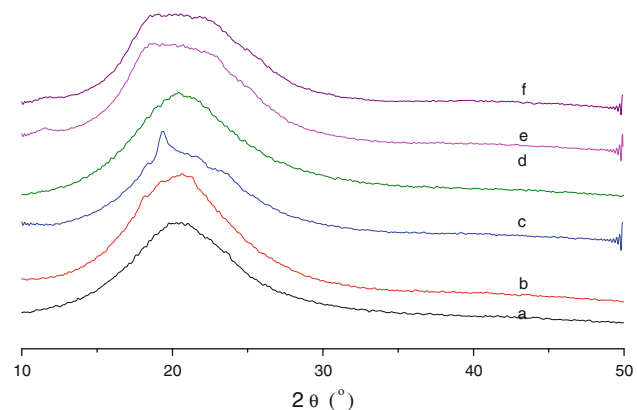


Fig. 3 WAXD traces of MB-PUPys with various MDI–BDO contents: **a** PUPyMB0; **b** PUPyMB15; **c** PUPyMB25; **d** PUPyMB35; **e** PUPyMB45; and **f** PUPyMB55

non-crystalline peak gets broader in the sample with higher MDI–BDO content. The peak width at half height is related to the domain size [37]. Thus, the enlargement of peak width reflects that the hard domain size becomes bigger with respect to the increase of MDI–BDO content. Hence, it is confirmed that the addition of MDI–BDO segment promotes the formation of hard domains in the BINA–HDI–BDO–MDI system.

DMA analysis

Figure 4 shows the DMA curves of MB-PUPys with various MDI–BDO contents. It is well known that MDI–BDO is the main composition of hard segment which is the physical netpoints of SMPU due to their strong interaction. They will probably lead to phase separation or hard domain formation and disperse among the soft segment phase as a filler to improve the mechanical properties of polyurethane [32]. Hence, it is observed in Fig. 4 that the glassy modulus (E_g) is higher than 3.5 GPa, while the rubber modulus (E_r) increases significantly with the increase of MDI–BDO content in the BINA–HDI–BDO–MDI system. As a result, the modulus ratio (E_g/E_r) decreases significantly with the increase of MDI–BDO content. The modulus ratio is changed from 548 in the PUPyMB0 to only 19 in the PUPyMB45. It is confirmed again that the phase-separation structure composed of soft phase and hard phase occurs in the BINA–HDI–BDO–MDI system; the addition of MDI–BDO segment reinforces the hard domains of MB-PUPys. In addition, it is also observed in Fig. 4b that the $\tan\delta$ drops significantly with respect to the increase of MDI–BDO content or the decrease of BINA content. This tendency is very similar to the tendency observed in the BINA–HDI–BDO system, in which the $\tan\delta$ drops with respect to the decrease of BINA content [29]. Hence, it is

confirmed again that the hydrogen bonding present in the pyridine ring does affect the energy loss of Py-SMPUs. It indicates that the MDI–BDO segment interrupts the energy loss of MB-PUPys, i.e., a lower MDI–BDO content or a higher BINA content PUPy tends to show higher energy loss during the glass transition process.

AFM analysis

In the previous literature, it was reported that phase separation occurs in the BINA–HDI–BDO system [27–29]. According to the DSC and DMA investigations above, it is found that the BINA–HDI–BDO–MDI system also has two phases, amorphous soft phase and amorphous hard phase. The phase-separation morphology can be inferred directly from AFM measurements [38]. Figure 5 presents the AFM images of PUPyMB0 (BINA–HDI system) and PUPyMB35 (BINA–HDI–BDO–MDI system). It is found in Fig. 5a that the PUPyMB0 contains soft phase (black area) and hard phase (white area). Moreover, the two phases are distributed homogeneously since the white area and black area both are not continuous in the AFM phase image. When the MDI–BDO segment is introduced, it is found in Fig. 5b that the domain of white area is enhanced. It indicates that the hard phase is increased in the BINA–HDI–BDO–MDI system. It is confirmed again that the addition of MDI–BDO segment promotes the formation of hard domain.

Shape memory behaviors

Thermal–mechanical properties

The important quantities to be determined for describing shape memory properties of materials are the shape recovery (R_r) and shape fixity (R_f). The shape recovery

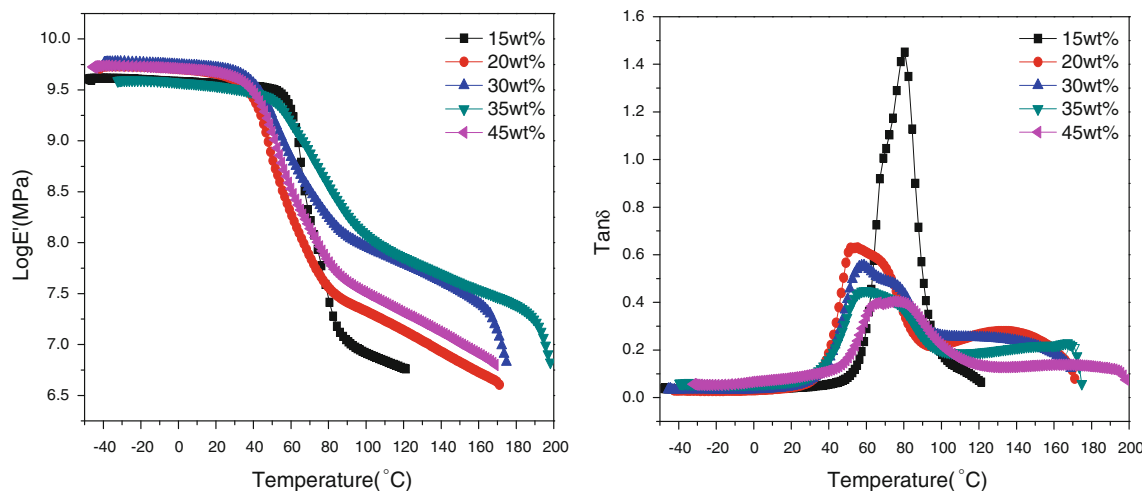
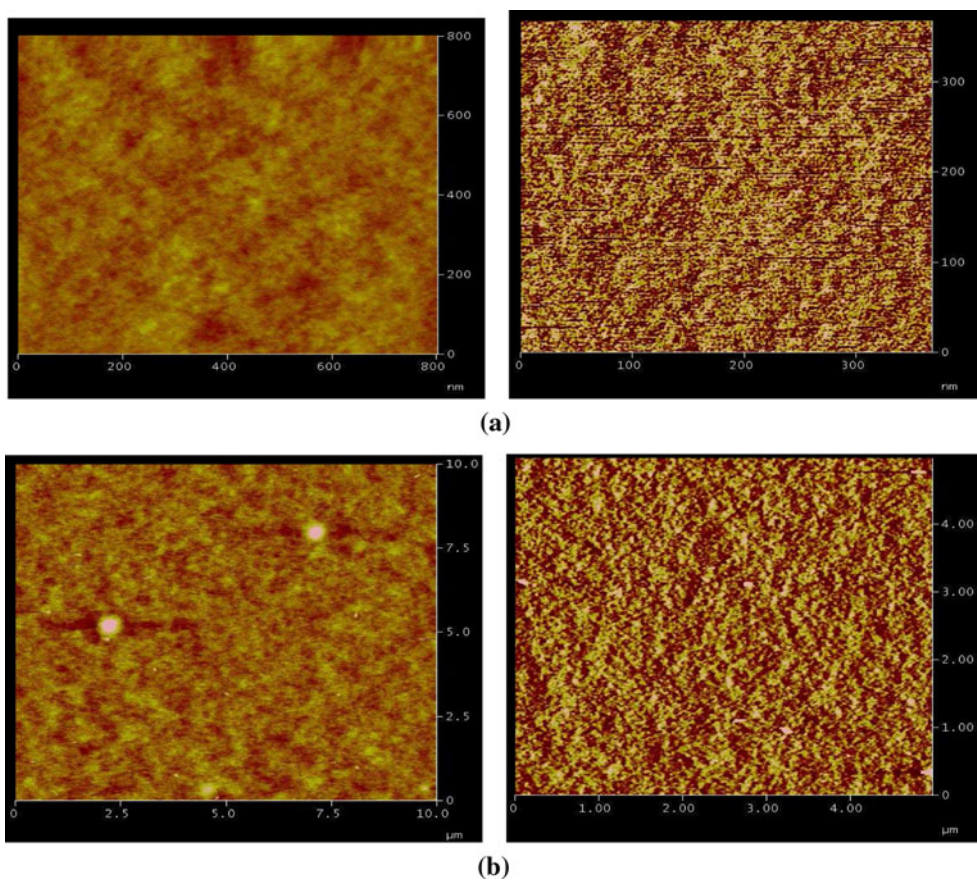


Fig. 4 DMA curves of MB-PUPys with various MDI–BDO contents

Fig. 5 AFM images of **a** PUPyMB0 and **b** PUPyMD35



qualifies the ability of SMPs to memorize its permanent shape, whereas the shape fixity describes the ability of switching segment to fix the mechanical deformation [29]. It was reported that both shape fixity and shape recovery were enhanced with respect to the increase of MDI–BDO content in the PTMG–MDI–BDO system of SMPUs [32]. The shape fixity increased with the increase of SSL but decreased with the increase of HSC; while, the shape recovery decreased with the increase of SSL and HSC when the HSC reaches a threshold value in the PHA-based-SMPU [12]. However, the structure and morphology of Py-SMPUs are different from the previous segmented SMPU since they contain only short chains with strong hydrogen bonding as described above. The shape memory behavior of Py-SMPUs should be different from the previous systems. In the earlier communication, shape memory behaviors of Py-SMPUs with various BINA contents have been investigated systematically. As compared with the common SMPU, the Py-SMPUs showed higher shape fixity. The shape recovery of Py-SMPUs decreased gradually as the BINA content decreases. The shape recovery was lower than 90% when the BINA content dropped below 30 wt% in the BINA–HDI–BDO system [29]. In addition, it is known that the hard segment, i.e., MDI–BDO, acting as the physical netpoints, is responsible for the strain recovery in the

traditional SMPU. Thus, it is necessary to investigate the shape memory behaviors and study the effect of MDI–BDO segment on SMEs of MDI–PUPys.

In the above analysis, it is known that the polar MDI–BDO segment reinforces the polarity of urethane unit due to their expected strong inter-molecular forces among the MDI–BDO segment in the BINA–HDI–BDO–MDI system. To understand the shape memory behavior of MB-PUPys, the thermal–mechanical testing was performed under the condition of 100% elongation at 45 °C, fixing at 20 °C, and recovering at 80 °C. Figure 6 presents the cyclic tensile curves of MB-PUPys with various MDI–BDO contents. It is observed that the addition of MDI–BDO content has little influence on the shape fixity of MB-PUPys. Even the PUPyMB55 which contains only 24.2 wt% BINA and 55 wt% MDI–BDO content still has shape fixity of 96.9%. It implies that the shape fixity is mainly determined by the glassy modulus. This is due to the fact that there are strong hydrogen bondings in the pyridine ring and urethane groups, and the movement of polymer strain is mainly controlled by these hydrogen bondings within the lower temperature range [30]. Therefore, though the modulus ratio is smaller, e.g., only 19 in the PUPyMB45, the higher glassy modulus (e.g., above 3.5 GPa) can fix more than 97% mechanical deformation (Table 2).

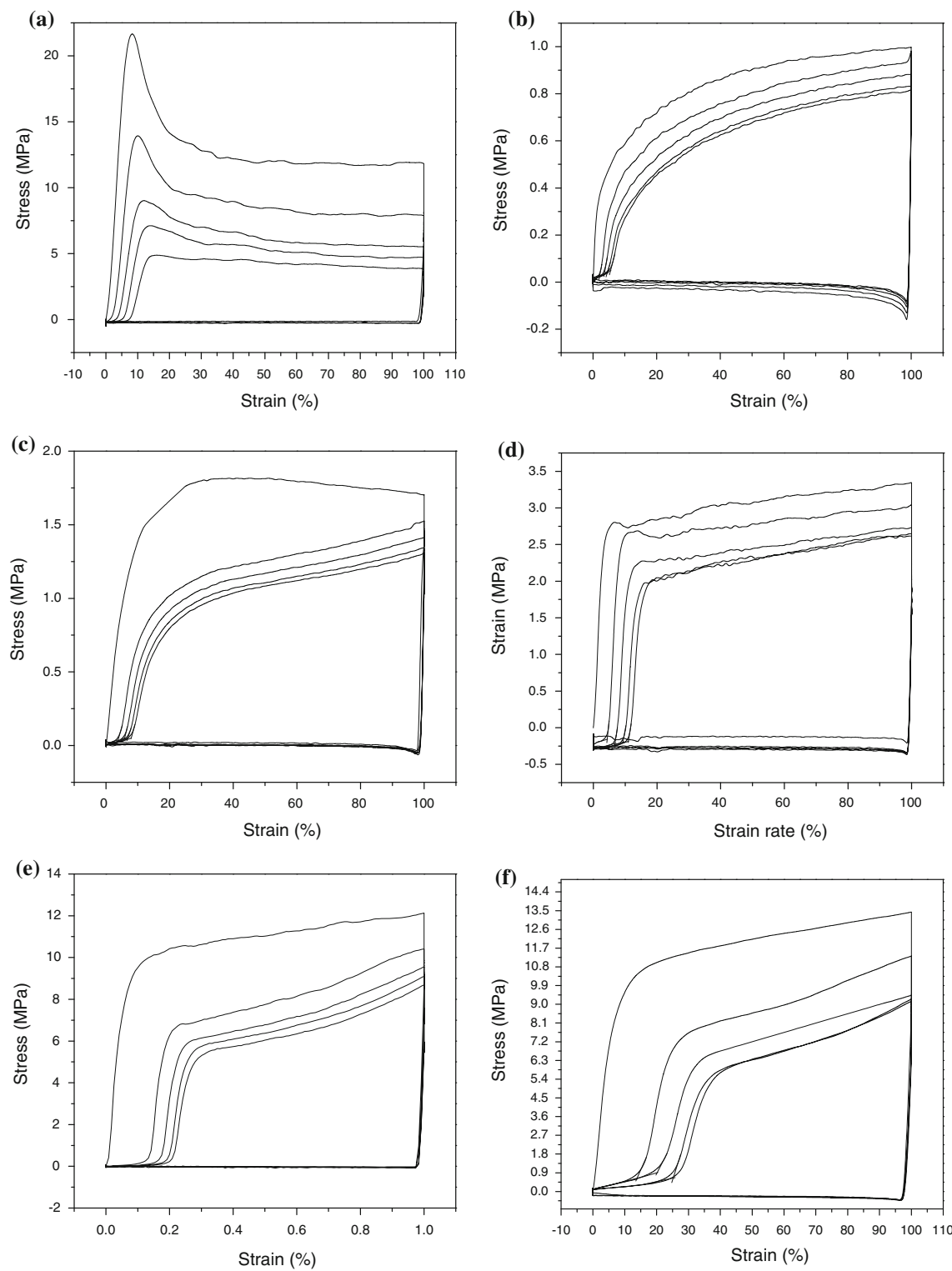


Fig. 6 Cyclic tensile curves of MB-PUPys with various MDI–BDO contents: **(a)** PUPyMB0, **(b)** PUPyMB15, **(c)** PUPyMB25, **(d)** PUPyMB35, **(e)** PUPyMB45, and **(f)** PUPyMB55

In addition, it is found in Fig. 6 that the shape recovery decreases with respect to the increase of MDI–BDO content or the decrease of BINA content. For example, the

PUPyMB35 having 35 wt% BINA and 35% MDI–BDO content shows a shape recovery of above 90% in the first three test cycles. However, when the MDI–BDO content is

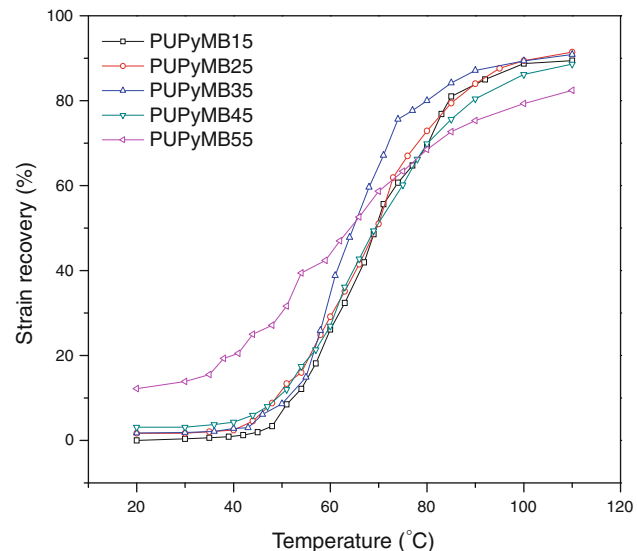
Table 2 Cyclic tensile testing results of MB-PUPys with various MDI–BDO contents

Samples	BINA wt%	MB wt%	R_f	1st R_r	2nd R_r	3rd R_r	4th R_r
PUPyMB0	53.7	0	98.4	98.54	96.34	94.49	92.57
PUPyMB15	45.5	15	98.6	97.91	96.44	94.45	94.43
PUPyMB25	40.3	25	98.0	96.17	94.08	93.16	92.09
PUPyMB35	34.9	35	98.6	95.70	93.12	90.64	88.99
PUPyMB45	29.5	45	97.4	86.65	82.88	80.41	78.85
PUPyMB55	24.2	55	96.9	86.33	79.81	74.68	73.02

increased to 45 wt% while still keeping the BINA content of 30 wt%, the shape recovery decreases to only about 79% after the fourth test cycle. This means that the addition of MDI–BDO segment does not influence the shape recovery in the BINA–HDI–BDO–MDI system. It might be due to the fact that the addition of MDI–BDO segment can only promote the formation of hard domains, and both the soft phase and hard phase are still distributed homogeneously in the BINA–HDI–BDO–MDI system, i.e., the addition of MDI–BDO segment does not influence the intensity and distribution of physical netpoints. Thus, the shape memory behaviors of MB-PUPys are mainly influenced by the BINA content, but not the MDI–BDO content.

Temperature-dependent strain recovery

Figure 7 presents the temperature-dependent strain recovery curves of MB-PUPys with various MDI–BDO contents. The temperature-dependent strain recovery curve is used to describe the change of strain recovery rate as a function of temperature upon heating process. Several parameters can be obtained from the recovery curve for describing the characteristic features of shape memory behavior of specimens [29]. For example, the final recovery rate (R_f) characterizes the recovery ability of the specimen. The temperature corresponding to a recovery rate value of $1/2R_f$ is called response temperature or average response temperature (T_r) of SMPs on the thermal recovery curve [17]. In the earlier communication, it was reported that the critical BINA content for Py-SMPUs exhibiting good SMEs is about 30 wt%. When the BINA content decreases to below 30 wt%, both the final recovery rate and shape fixity are unacceptable [29]. Similarly, it is found in Fig. 7 that the MB-PUPys also show the typical S-shaped strain recovery process. The shape changes slightly below the initial temperature (T_i), e.g., 45 °C, in the PUPyMB15. However, when the temperature is raised to above T_i , the deformed strain starts to recover, significant strain recovery being observed within the temperature range of 50–70 °C. Hence, the T_r is about 65 °C in the PUPyMB15. When the temperature is raised above the end temperature, e.g.,

**Fig. 7** Strain recovery curves of MB-PUPys with various MDI–BDO contents

85 °C, more than 90% deformed strain is recovered. The similar shape recovery process is also found in the PUPyMB15, PUPyMB25, PUPyMB35, and PUPyMB45. The shape fixity is beyond 95%, and the final shape recovery is approximately 90% at 110 °C. It shows that they all have good thermal-induced SME. However, when the MDI–BDO content is higher than 55 wt%, or the BINA content is lower than 25 wt%, it is observed in Fig. 7 that the PUPyMB55 has the shape fixity of less than 89%, and shape recovery of less than 82%. The strain is recovered gradually with respect to the increase of temperature. It implies that the shape fixity and the shape recovery tend to drop significantly when the MDI–BDO content is higher than 55 wt% in the BINA–HDI–BDO–MDI system. However, as for the BINA content which drops to less than 25 wt% in the PUPyMB55, this result is still consistent with change tendency of shape recovery observed in the BINA–HDI–BDO system [29]. It is confirmed again that the BINA unit is the main composition influencing the thermal-induced SME of Py-SMPUs, i.e., high shape fixity and shape recovery can be achieved if the BINA content is kept above 30 wt% in the BINA–HDI–BDO–MDI system. The addition of MDI–BDO segment does not influence the shape memory behaviors of Py-SMPUs.

Strain recovery force

The recovery energy can be stored in the deformed shape, and the restoration force is considered as an important factor for the SMPs. It is proposed that the restoration force of SMPs can be measured as the temperature increases from room temperature to the higher temperature (above T_r) by fixing the specimen length after a procedure of deformation

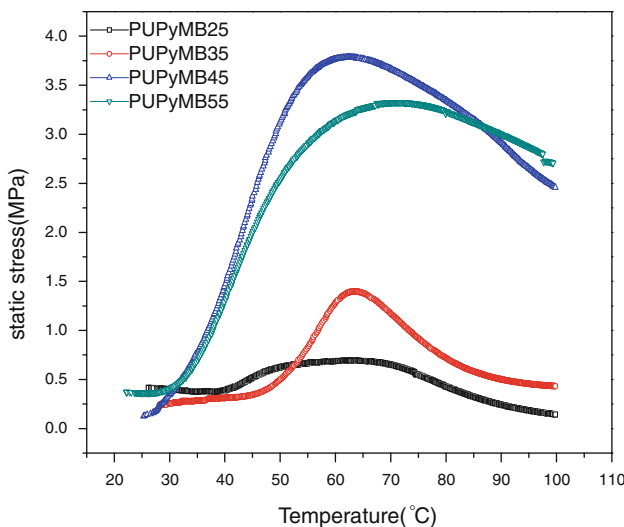


Fig. 8 Static stress curves of BIN–SMPU with various MDI–BDO contents

and fixation [29, 39]. In the earlier report, it was found that the static stress existed in the PUPyMB0 does not appear until the temperature was raised to above 43 °C, and the maximum value was observed at about 50 °C. The static stress was kept within the temperature of 50–58 °C, and it decreased with respect to the increase of temperature above 58 °C. Comparatively, it was found that the maximum value of static stress increased significantly with respect to the decrease of BINA content [29]. In this study, the static stress is recorded to characterize the restoration force upon heating using the DMA by controlling the displacement to a very small value, e.g., 0.001 mm. Figure 8 presents the static stress curves of MB-PUPys with various MDI–BDO contents under the elongation of 100%. Similar to the observation in the BINA–HDI–BDO system, there is little static stress in the PUPyMB35 before 47°. The static stress increases to its maximum value of 1.4 MPa when the temperature is raised to above 47°, but it will decrease to a very small value above 100°. In addition, it is also observed in Fig. 8 that the MB-PUPys with the higher MDI–BDO content sample, e.g., PUPyMB55, tends to show a higher static stress in the BINA–HDI–BDO–MDI system. This is due to the fact that the higher MDI–BDO content has higher rubber modulus as described in DMA analysis; the driving force for shape recovery in a polymer is the elastic strain generated during the deformation [29]. Thus, it is confirmed that the addition of MDI–BDO segment reinforces the hard phase, improving the shape recovery force.

Conclusions

In this article, a series of MB-PUPys with various MDI–BDO contents are synthesized from HDI, BINA, BDO, and

MDI. After investigations with FT-IR, DSC, DMA, WAXD, and shape memory testing, the following conclusions can be summarized.

1. The addition of MDI–BDO segment improves the strength of hydrogen bonding of urethane groups of MB-PUPys.
2. The addition of MDI–BDO segment does promote the formation of hard domains, but it does not influence the phase-separation structure of MB-PUPys. Amorphous soft phase and amorphous hard phase occur in the BINA–HDI–BDO–MDI system. However, the addition of MDI–BDO segment does not influence the intensity and distribution of physical netpoints.
3. The MDI–BDO segment improves the rubber modulus and interrupts the energy loss of MB-PUPys, i.e., the rubber modulus increases with the increase of MDI–BDO content, and a lower MDI–BDO content sample tends to show higher energy loss during the glass transition process.
4. The addition of MDI–BDO segment does not influence the shape memory behaviors which are mainly influenced by the BINA content. If the BINA content is kept above 30 wt%, high shape fixity and shape recovery can be achieved in the BINA–HDI–BDO–MDI system; and a higher shape recovery force can be obtained by increasing the MDI–BDO segment.

Acknowledgements This study was financially supported from the Natural Science Foundation of China (No. 50803037), Natural Science Foundation of Guangdong (No. 2008211), and the PhD studentship of Hong Kong Polytechnic University. The authors also would like to thank Prof. Jean-Marie Lehn, the Nobel Prize Laureate in 1987, for his guidance.

References

1. Nji J, Li GQ (2010) Polymer 51:6021
2. Zhang H, Wang HT, Zhong W, Du QG (2009) Polymer 50:1596
3. Behl M, Razzaq MY, Lendlein A (2010) Adv Eng Mater 22:3388
4. Meng H, Hu JL (2010) J Intell Mater Syst Struct 21:859
5. Hu JL, Chen SJ (2010) J Mater Chem 20:3346
6. Yang D, Huang W, Yu JH, Jiang JS, Zhang LY, Xie MR (2010) Polymer 51:5100
7. Ji FL, Hu JL, Li TC, Wong YW (2007) Polymer 48:5133
8. Wang XH, Zhang W, Lan X, Liu YJ, Leng JS (2007) Basic properties and application of shape memory polymer composite to deployable hinge for solar arrays. International Conference on Smart Materials and Nanotechnology in Engineering, Pts 1–3 6423:42356–42356. doi:[10.1117/12.780331](https://doi.org/10.1117/12.780331)
9. Chen SJ, Cao Q, Liu PS (2006) Acta Polym Sin 1:1
10. Chen SJ, Cao Q, Jing B, Cai YL, Liu PS, Hu JL (2006) J Appl Polym Sci 102:5224
11. Zhuo HT, Hu JL, Chen SJ, Yeung LP (2008) J Appl Polym Sci 109:406
12. Chen SJ, Hu JL, Liu YQ, Liem HM, Zhu Y, Liu YJ (2007) J Polym Sci Polym Phys 45:444

13. Chen SJ, Hu JL, Zhuo HT, Zhu Y (2008) Mater Lett 62:4088
14. Zhuo HT, Hu JL, Chen SJ (2008) Mater Lett 62:2078
15. Chen SJ, Hu JL, Liu YQ, Liem HM, Zhu Y, Meng QH (2007) Polym Int 56:1128
16. Kim BK (1999) Appl Mech Eng 4:435
17. Li FK, Hou JN, Zhu W, Zhang X, Xu M, Luo XL, Ma DZ, Kim BK (1996) J Appl Polym Sci 62:631
18. Chun BC, Chong MH, Chung YC (2007) J Mater Sci 42:6524. doi:[10.1007/s10853-007-1568-z](https://doi.org/10.1007/s10853-007-1568-z)
19. Mondal S, Hu JL (2007) J Elast Plast 39:81
20. Ping P, Wang WS, Chen XS, Jing XB (2007) J Polym Sci Polym Phys 45:557
21. Wang WS, Ping P, Chen XS, Jing XB (2007) Polym Int 56:840
22. Zhu Y, Hu J, Yeung K (2009) Acta Biomater 5:3346
23. Zhang S, Yu ZJ, Govender T, Luo HY, Li BJ (2008) Polymer 49:3205
24. Li JH, Viveros JA, Wrue MH, Anthamatten M (2007) Adv Eng Mater 19:2851
25. Luo HY, Liu Y, Yu ZJ, Zhang S, Li BJ (2008) Biomacromolecules 9:2573
26. Zhu Y, Hu JL, Liu YJ (2009) Eur Phys J E 28:3
27. Chen SJ, Hu JL, Yuen CWM, Chan LK (2009) Mater Lett 63:1462
28. Chen SJ, Hu JL, Yuen CWM, Chan LK (2009) Polymer 50:4424
29. Chen SJ, Hu JL, Zhuo HT, Yuen CWM, Chan LK (2010) Polymer 51:240
30. Chen SJ, Hu JL, Yuen CWM, Chan LK (2010) Polym Int 59:529
31. Zhang CL, Hu JL, Chen SJ, Ji FL (2010) J Mol Model 16:1391
32. Lee BS, Chun BC, Chung YC, Sul KI, Cho JW (2001) Macromolecules 34:6431
33. Ratna D, Karger-Kocsis J (2008) J Mater Sci 43:254. doi:[10.1007/s10853-007-2176-7](https://doi.org/10.1007/s10853-007-2176-7)
34. Cao Q, Chen SJ, Hu JL, Liu PS (2007) J Appl Polym Sci 106:993
35. Robert WS, Stuart LC (1973) Macromolecules 6:48
36. Wang WS, Ping P, Chen XS, Jing XB (2006) Eur Polym J 42:1240
37. Zhou J, Wang HJ (2003) Chin J Geochem 22:1
38. Cao Q, Liu PS (2006) Polym Bull 57:889
39. Ping P, Wang WS, Chen XS, Jing XB (2005) Biomacromolecules 6:587